Journal of Molecular Structure 917 (2009) 148–157

Contents lists available at ScienceDirect

Journal of Molecular Structure

journal homepage: www.elsevier.com/locate/molstruc

Dual emission from (*E*)-3-(4-methylamino-phenyl)-acrylic acid ethyl ester (MAPAEE) and its application as fluorescence probe for studying micellar and protein microenvironment

Amrita Chakraborty [a], Shalini Ghosh [a], Samiran Kar [a,1], D.N. Nath [b], Nikhil Guchhait [a,*]

[a] Department of Chemistry, University of Calcutta, 92, A.P.C. Road, Kolkata 700009, India
[b] Department of Physical Chemistry, Indian Association for the Cultivation of Science Jadavpur, Kolkata 700 032, India

ARTICLE INFO

Article history:
Received 24 April 2008
Received in revised form 7 July 2008
Accepted 10 July 2008
Available online 19 July 2008

Keywords:
(*E*)-3-(4-Methylamino-phenyl)-acrylic acid ethyl ester
Dual emission
Twisted intramolecular charge transfer
TDDFT
Bovine serum albumin
Sodium dodecyl sulphate

ABSTRACT

Steady state absorption, fluorescence and time resolved fluorescence spectroscopy have been used for studying the photoinduced intramolecular charge transfer reaction in (*E*)-3-(4-methylamino-phenyl)-acrylic acid ethyl ester (MAPAEE). The title molecule shows dual emission due to high energy local and a low energy charge transfer emission. Depending on the nature of solvent the red shifted emission band shows good correlation with the solvent polarity parameter, $E_T(30)$ parameter and hydrogen bonding parameter. Quantum chemicals calculations by density functional theory predict that a stabilized twisted intramolecular charge transfer excited state generated either by twisting of the donor group (—NHMe) or the acceptor (- = —COOEt) group is responsible for the red shifted charge transfer emission. The solvent polarity dependent red shifted emission from the excited charge transfer state of MAPAEE has been used as fluorosensor to study bovine serum albumin proteinous and sodium dodecyl sulphate micellar microenvironment.

1. Introduction

Intramolecular charge transfer reactions in donor–acceptor substituted aromatic systems have been studied vastly by different groups due to its wide applications. In this process, the charge distribution takes place between the donor and the acceptor group by photoexcitation which leads to an increase of the dipole moment and as well as to structural and electronic rearrangements within the molecules. Lippert et al. [1] first reported the dual fluorescence of the benchmark molecule *N*,*N*-dimethylamino benzonitrile (DMABN) and assigned the higher energy emission band to normal emission of benzene like derivative and the 'anomalous', long wavelength, solvent dependent emission to highly polar, charge transfer (CT) emission. There are various proposed models, e.g., twisted intramolecular charge transfer (TICT), planar intramolecular charge transfer (PICT), wagged intramolecular charge transfer (WICT) and rehybridisation intramolecular charge transfer (RICT) for explaining this dual fluorescence phenomenon of DMABN [2–5], but the TICT model pioneered by Grabowski and coworkers [2] has received wide spread attention.

In this paper, we have demonstrated the photophysical properties of (*E*)-3-(4-methylamino-phenyl)-acrylic acid ethyl ester (Scheme 1) in different polarity solvents. The molecule MAPAEE contains a secondary amino group as charge donor (—NHMe) and ethyl ester (—COOEt) as charge acceptor with an extra π-conjugation between the benzene ring and the acceptor group. The studies of secondary amino group as charge donor for photoinduced intramolecular charge transfer reaction are very uncommon [6–8]. It is found that secondary amino donor group mainly shows CT emission when there is an *ortho* substitution in the ring of the chromophore [2]. Recently, Zachariasse et al. reported similar type of dual fluorescence for photoinduced intramolecular charge transfer (ICT) reaction of some secondary amino donor aromatics where fluorine atoms are substituted in the aromatic ring [8]. Very recently, we have reported photophysical phenomenon of some aromatic compounds with flexible double bond at the acceptor site and secondary amino group without ortho substitution at the donor site [9–11].We have earlier reported dual fluorescence phenomena in some self designed donor–acceptor aromatic systems where secondary amino group without ortho substitution was used as charge donor with variety of acceptor groups such as nitrile, aldehyde, acid, methyl ester groups. In the present study, the donor is a secondary amine and the acceptor is an ethyl ester. We found that the change of ester group from methyl to ethyl hardly influences the excited state CT reaction. We have studied photophysical proper-

* Corresponding author. Tel.: +91 33 2432 4159; fax: +91 33 2351 9755.
E-mail address: nguchhait@yahoo.com (N. Guchhait).
[1] Present address: CHEMGEN Pharma International, Dr. Siemens Street, Block GP, Sect. V, Salt Lake City, Kolkata 700 091, India.

0022-2860/$ - see front matter © 2008 Elsevier B.V. All rights reserved.
doi:10.1016/j.molstruc.2008.07.007

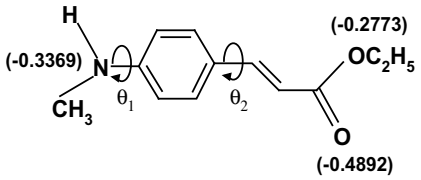

Scheme 1. Structure of (*E*)-3-(4-metylamino-phenyl)-acrylic acid ethyl ester. Calculated Mullikan charge given in parentheses.

ties of MAPAEE by varying polarity and hydrogen bonding ability of the solvent, pH and temperature of the medium. Theoretical potential energy surfaces at density functional theory (DFT) level for the lower singlet states of MAPAEE have been evaluated as a function of twisting coordinate along both the donor and acceptor sides [12]. The effects of solvent on spectral properties have been explored using polarizable continuum model (PCM) included in the Time dependent density functional theory (TDDFT) method [13]. Systems demonstrating ICT are recently being widely used as fluorosensors of microenvironment in proteins and micelles. Since the photophysical properties of MAPAEE were found to be dependant on the solvent polarities, an effort has also been made to study the interaction of MAPAEE with protein bovine serum albumin (BSA) and surfactant sodium dodecyl sulphate (SDS) for the study of proteinous and micellar microenvironments.

2. Experimental

For the synthesis of MAPAEE, *p*-nitro benzaldehyde and ethyl (triphenyl phosphanylidine)acetate ($Ph_3P{=}CH{-}COOEt$) in dry dichloromethane were stirred at room temperature for 24 h. Generated nitro product was reduced by zinc and saturated aqueous ammonium chloride solution in methanol at 50 °C for 30 minutes to produce (*E*)-3-(4-amino-phenyl)-acrylic acid ethyl ester. Then one hydrogen atom of amino group was blocked by di-*tert*-butyl pyrocarbonate (BOC-anhydride) in presence of triethylamine in THF to produce (*E*)-3-(4-amino-phenyl)-acrylic acid. In the next step, hydrogen atom of BOC protected amino group was replaced by methyl group using methyliodide in presence of sodium hydride base in DMF solvent at 0 °C. In the next step, the BOC group was removed by using trifluoroacetic acid in dichloromethane to produce (*E*)-3-(4-metylamino-phenyl)-acrylic acid ethyl ester. The final product was purified by column chromatography and repeated crystallization. ^{1}H NMR (300 MHz, $CDCl_3$) δ 1.29 (t, 3H), 2.86 (s, 3H), 4.19 (q, 2H), 6.18 (d, J = 11.85 Hz, 1H), 6.54 (d, J = 6.51 Hz, 2H), 7.35 (d, J = 6.48 Hz, 2H), 7.57 (d, J = 11.91 Hz, 1H).

The absorption and emission spectra of MAPAEE in different solvents have been measured by Hitachi UV/VIS U-3501 spectrophotometer and Perkin-Elmer LS50B fluorimeter, respectively. Solvents used for all measurements are spectral grade from Spectrochem and E-Mark. The protein BSA and surfactant SDS from SRL, India, were used for the preparation of proteinous and micellar solution. All solutions are made at $\sim 10^{-6}$ M concentration of solute in order to avoid aggregation and self-quenching.

The time resolved fluorescence measurements have been done with a time correlated single photon counting set up. The exciting source is frequency tripled output of mode locked picosecond Ti-Sapphire Tsunami (Spectra Physics, USA) laser pumped by a diode pumped CW Nd-Vanadate laser (Millenia X, Spectra Physics, USA). For our measurement the excitation wavelength is 315 nm. A pulse repetition rate of 82 MHz has been reduced to a repetition rate of 800 kHz/4 MHz by a pulse selector. The average power is in between 2 and 50 mW. The instrument response function (IRF) is 20 ps. The time interval between the exciting photon (laser pulse) and a single fluorescence photon from the fluorescent sample excited by the same laser pulse has been measured in repeated cycles and the data has been used to construct fluorescence decay of the sample. The 345 nm filter has been used for removing the scatter light. The instrument response function (IRF) has been measured by using a scattering solution of milk powder in water.

All calculations have been performed using Gaussian 03 package [19]. The geometries of the ground state lowest energy conformers have been calculated with B3LYP hybrid functional and 6-31++G(d,p) basis set at DFT level. Time dependent density functional theory (TDDFT) has been used to calculate excitation energies using the same functional and basis set. In spite of certain drawbacks [14,15,21], there are various examples where TDDFT has been used successfully to explore photophysical phenomena for the ground and excited states [9–12,16–18,20]. Computed excitation energies are the vertical transition energy without zero point correction. We also extended our calculations in solvated system using non-equilibrium TDDFT–PCM model [17]. Calculations on potential energy surface (PES) have been pursued along the twist coordinates separately at the donor and acceptor sites. We have used rotational angles θ_1 and θ_2 (shown in Scheme 1) to get the twisting of the donor (—NHMe) and acceptor (—CH=CHCOOEt) group, respectively. One limitation is that the above-calculated PES only corresponds to the cut of PE-hyper surface along the twisting angle as no geometry optimization of the various excited states has been performed. However, this approach, i.e., the use of ground state optimized geometry as a basis for the representation of the excited state structure, has been successfully applied in many recent scientific publications [16–18,22]. The difference in energy between the S_0 and S_1 or S_2 states of the calculated PESs without optimization of the excited states at different twisted geometry is considered as the emission energy [17]. This value is just an estimation of the emission energy but not a theoretical estimation of vertical emission from the excited state since the excited state optimization has not been considered.

3. Results and discussion

3.1. Absorption spectra

The absorption spectra of MAPAEE in a series of polar, non-polar and protic solvents have been measured and the positions of the band maxima are presented in Table 1. The absorption spectra in non-polar and polar aprotic solvents show a broad band consisting

Table 1
Absorption and emission spectral data of MAPAEE in different solvents at room temperature

Solvent	λ_{abs} (nm)	λ_{flu} (nm)	ν_{abs} (cm^{-1})	ν_{flu} (cm^{-1})	$\Delta\nu$ (cm^{-1})
Hexane	333, 318	382	30,030	26,178	3852
Dioxane	350, 318	413	28,571	24,213	4358
Chloroform	351, 318	418	28,490	23,923	4567
Tetrahydrofuran	352, 318	422	28,409	23,696	4712
Acetonitrile	353, 318	435	28,328	22,988	5501
Ethanol	358, 318	443	27,932	22,573	5359
Methanol	359, 318	454	27,855	22,026	5828
Water	346, 318	467	28,901	21,413	7488

of two overlapping bands, a strong band at ~350 nm and a weak shoulder one at ~318 nm (Fig. 1a). The spectral pattern is similar to that of (*E*)-3-(4-methylamino-phenyl)-acrylic acid methyl ester (MAPAME), a methyl ester of the same molecule [13]. The conjugated double bond and a secondary amino group attached to the benzene ring, results in the red shift of the strong π–π^* band to 350 nm due to resonance stabilization. It is found that the peak position of the low energy band varies slightly with solvent polarity; but the position of the high energy band is independent of solvent polarity. Comparing with methyl analogue MAPAME and other similar studied systems these two absorption bands are assigned to transition to $L_a(S_2)$ and $L_b(S_1)$ state of benzene moiety [11,12,23]. In protic solvent like water the strong absorption band (346 nm) is slightly blue shifted and the shifting is such that the two bands almost overlap to produce a single absorption peak. As was observed for similar donor–acceptor systems, this blue shifted band corresponds to the hydrated clusters of MAPAEE [9–11,24–26]. In the ground state protic solvents act as proton donor and can form the possible hydrogen bonded clusters (Scheme 2). It is found that specific hydrogen bonding is an important factor to favour the ICT process by maintaining a large twist angle between the electron donor and acceptor group in the ground state [25]. Stabilization of ground state through hydrogen bonding can shift the absorption band to the blue side.

The absorption spectra in presence of acid are shown in Fig. 1b. With increase of acidity of the medium the absorption band in methanol shifts more towards blue side from ~347 nm to ~270 nm. Obviously the H^+ ion of acid prefers to bind to electronegative atoms to form a protonated species which absorbs at ~270 nm. The possible protonation sites are two oxygen atoms and one nitrogen atom and the calculated negative charge density at nitrogen atom and two oxygen atoms for the lowest energy structure support this prediction (Scheme 1). The π–π^* type of absorption of such protonated species is similar to that of benzene chromophore having only a conjugated double bond and therefore, this protonated species should absorbed at the blue side due to less resonance stabilization compared to the neutral species.

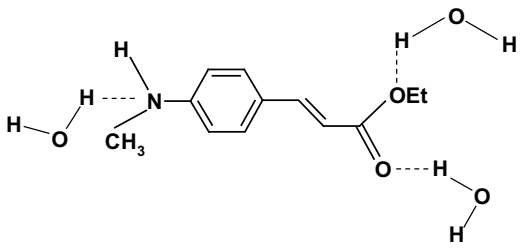

Scheme 2. Structure of hydrated cluster of (*E*)-3-(4-metylamino-phenyl)-acrylic acid ethyl ester.

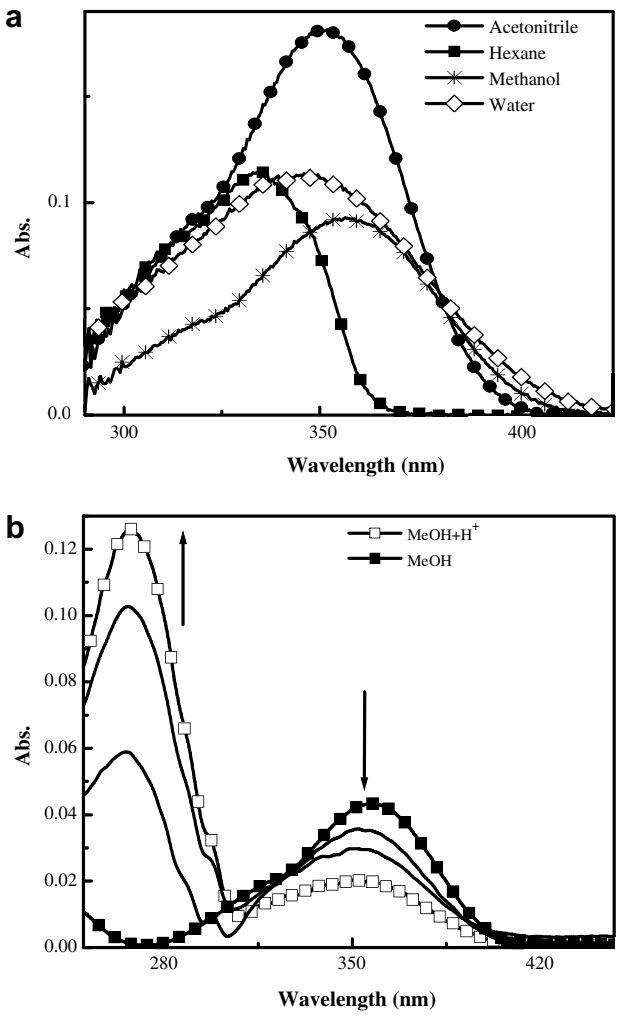

Fig. 1. Absorption spectra of MAPAEE in (a) different solvents, (b) in presence of acid (arrow indicates increase of acid concentration).

3.2. Emission spectra

Fig. 2 shows the emission spectra of MAPAEE in some selective solvents when excited at the absorption band maxima. The emission peaks in different solvents are presented in Table 1. It is found that the emission spectra MAPAEE are similar to the emission spectra of its methyl analogue MAPAME [11]. As seen in Fig. 2a, a strong red shifted fluorescence band is observed with increasing polarity and hydrogen bonding ability of the solvents. Comparing with other similar reported molecules [9–11] we have assigned the large red shifted emission in polar aprotic solvent to emission from the CT state and higher energy emission band to local emission. In polar solvents the higher energy emission band is broad enough with high base line value and considered to be the emission from a locally excited state of the molecule. The lower energy, Stokes shifted emission band may arise from CT state generated from the hydrogen bonded clusters in protic solvent [26]. It is reported that intermolecular hydrogen bonding effect is an interesting subject to determine proton coupled charge transfer process which is observed in biological assembles including PS II systems [27]. As seen in Fig. 2b, the addition of little amount of ethanol in methylcyclohexane solution of MAPAEE shows the generation of new fluorescence band at the red side with concomitant decrease of initial emission band observed in pure methylcyclohexane. A clear isoemissive point at ~398 nm characterizes the excited state hydrogen bonding complex formation of simple stoichiometry with protic solvents [25,28]. As was seen in case of methyl analogue the excitation spectra of MAPAEE (figure not shown) of both the emission bands are independent of emission wavelength and agree reasonably well with the absorption spectra indicates that only a single species is present in the ground state and hence the CT state generated from the LE state.

As was observed in the absorption spectra, the emission in methanol is also found to be pH dependent (Fig. 2c). With increasing the acidity of the medium, the intensity of charge transfer (CT) emission band decreases with increase of intensity of a locally excited (LE) state emission band of the possible protonated species. As the proton prefers to bind to the nitrogen lone pair, the lone pair of nitrogen is now not available for intramolecular charge transfer reaction; hence the CT band intensity decreases with increasing acid concentration. Surprisingly, this charge transfer band does

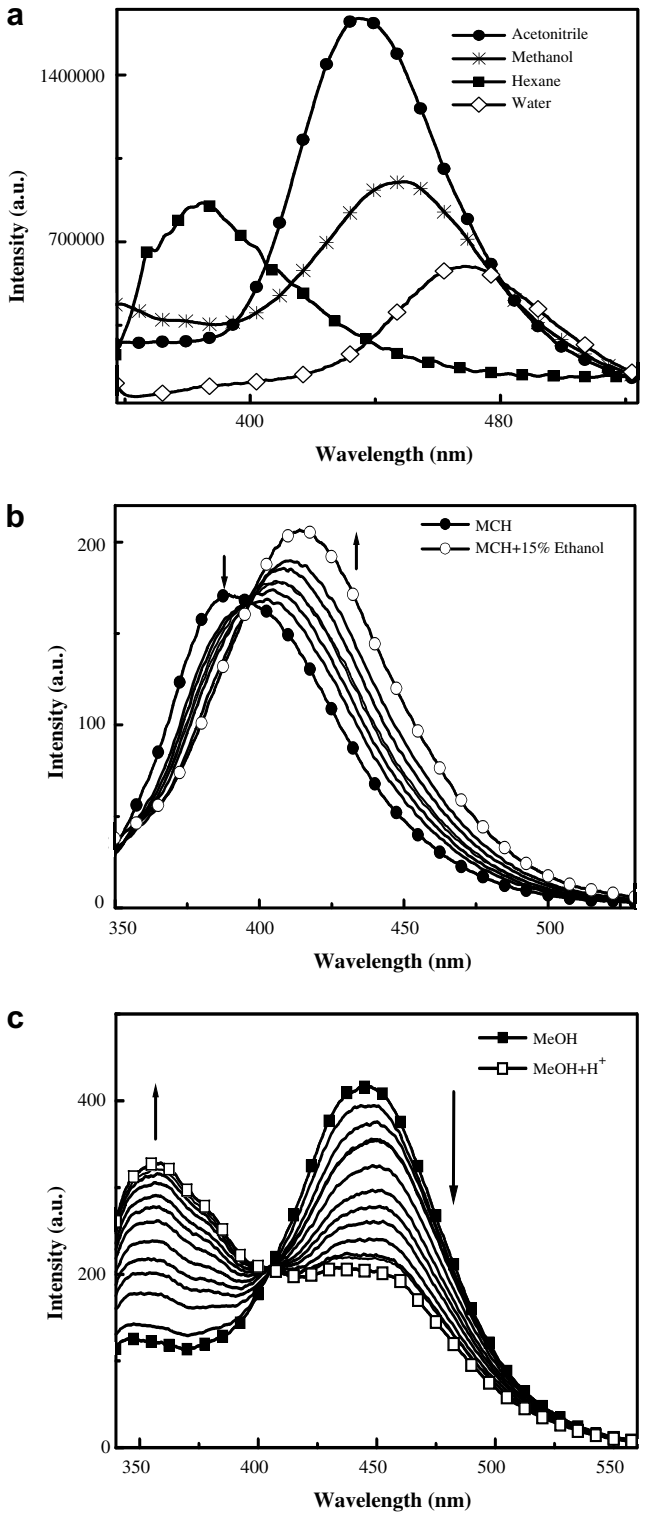

Fig. 2. Emission spectra of MAPAEE in (a) different polarity solvents, (λ_{ext} = 340 nm), (b) in methylcyclohexane + ethanol mixed solvent and (c) in presence of acid (arrow indicates increase of acid concentration) (λ_{ext} = 270 nm).

not totally disappear even in high acid concentration and both the LE of the protonated species and CT band coexist. This can be possible if the LE state of the protonated species can undergo excited state deprotonation reaction to some extent [29]. The deprotonated excited state immediately transforms to the CT state in the excited state potential energy surface, hence both the emission of the protonated species and the CT state appears in highly acidic medium. The effect of acid on the absorption and emission spectra predicts that the CT state is generated from the transfer of charge from the lone pair of nitrogen atom. From the absorption and emission spectra of MAPAEE, it is observed that the overall spectral characteristics of MAPAEE are similar to that of MAPAME. Hence, the change of substituents of the acceptor ester group does not affect spectral characteristics at all.

To determine the excited state dipole moment of MAPAEE we have used Lippert plot from the data obtained from absorption and emission spectra [30].

$$\overline{\nu}_a - \overline{\nu}_f = \left[\frac{2}{hca^3}\right]\Delta f[\mu^* - \mu]^2 + cons\tan t$$

$$\text{where, } \Delta f = \left[\frac{\varepsilon - 1}{2\varepsilon + 1}\right] - \left[\frac{n^2 - 1}{2n^2 + 1}\right]$$

In the above equation h, c, a, μ and μ^* are the Planck's constant, velocity of light, radius of the cavity in which the fluorophore resides and ground and excited CT state dipole moments, respectively. The term Δf is known as solvent polarity parameter and ε and n are the dielectric constant and refractive index, respectively, of the medium. The ground state dipole moment (μ) and 'a' values were calculated using hybrid functional B3LYP and 6-31++G(d,p) basis set for the ground state minimum energy structure and the values are 5.39 D and 4.5 Å, respectively. Fig. 3a shows a linear dependency of Stokes shift on solvent polarity parameter. High dipole moment of excited CT state (9.8 D) calculated by solvatochromic method again confirms the charge transfer nature of the excited state.

The large deviation from linearity in Lippert plot in case of protic solvent indicates that hydrogen bonding may play a key role in ICT path. As seen in Fig. 3b, the correlation of Stokes shift with solvent dependent properties $E_T(30)$ parameter [31] follows two distinct lines, one for the non-protic solvents and the other for the protic solvents. This clearly indicates the presence hydrogen bonding interaction along with the dipolar interaction in polar protic solvents. A linear correlation between the lower energy emission band maximum and hydrogen bonding parameter (α) [32] of protic solvents again supports the fact (Fig. 3c) that hydrogen bonding causes preferential solvation of ICT state by lowering its energy value and facilitate CT process in the excited state. The measurements of luminescence quantum yield and excited state depopulation kinetics data are collected in Table 2. With the help of excited state lifetimes and quantum yields it is possible to calculate both the radiative decay rate constant (k_f) and the sum of the rate constants of parallel non-radiative processes (k_{nr}). The values of k_f and k_{nr} are calculated by the following equations [28].

$$k_f = \phi_f/\tau_f \quad \text{and} \quad k_{nr} = (1/\tau_f) - k_f$$

Fluorescence quantum yields are quenched by protic solvents compared to polar aprotic solvents. In protic solvents the quantum yields value decrease with increasing α parameters, describing the acidity of the hydrogen bonding solvents. This indicates the existence of non-radiative decay channels of increasing importance with growing proton donating ability of the solvent. In hexane, MAPAEE shows a very short fluorescence lifetime value of ~12 ps, even lower than the IRF (20 ps). The high non-radiative rate in hexane indicates that additional radiationless channels may be present in non-polar solvent as was observed by Maus et al. [33]. With increasing the polarity of the medium, i.e., in acetonitrile solvent the lifetime value increases to 27 ps with a negative component of small contribution. We are not sure about this growth. The higher radiative rate in acetonitrile with respect to hexane can be explained by considering the fact that with increasing the polarity of the medium the CT state become more stabilized leading to less

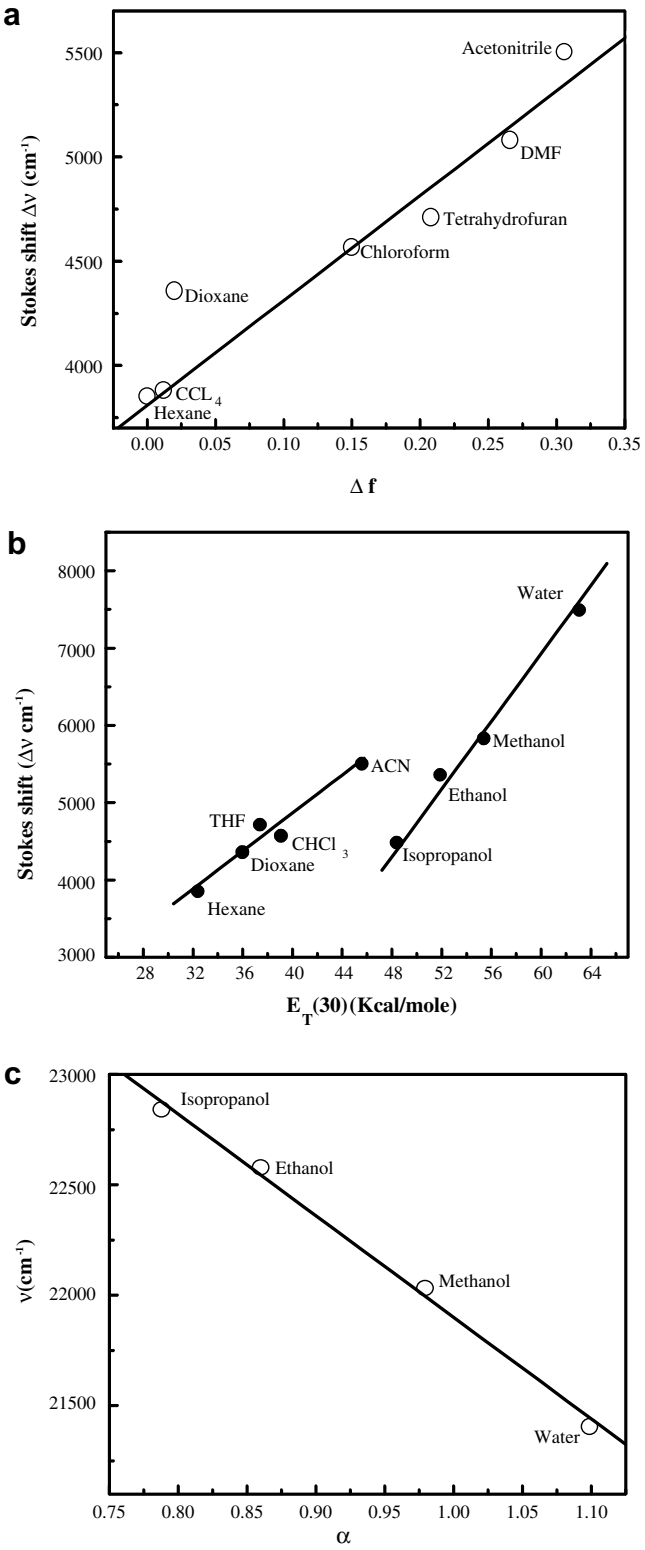

Fig. 3. (a) Plot of Stokes shift vs. solvent parameter (Δf) (Lippert plot) of MAPAEE, (b) Plot of Stokes shift vs. $E_T(30)$ parameter and (c) plot of fluorescence band maximum of MAPAEE vs. hydrogen bonding parameter (α).

mixing with the forbidden L_b type state. In methanol solvent the lowering of fluorescence lifetime value and increase of non-radiative rate constant with respect to acetonitrile solvent again support that hydrogen bonding acts as non-radiative path in ICT reaction.

The emission of MAPAEE in ethanol glass matrix is shown in Fig. 4. The emission band maximum at 77 K is found to be largely blue shifted. This may reflect the change in solvent properties such as polarity, polarizability and viscosity upon decreasing the temperature. The high viscosity of the 77 K glass matrix also inhibits the relaxation process from LE to CT state through any expected twisting path. Hence only LE emission should be observed in low temperature glass matrix. This observation may support the proposed mechanism of TICT where twisting of either the donor or acceptor side are responsible for red shifted emission band [34,9,10].

3.3. Theoretical calculation

To get a better insight into the excited state processes we have performed structural calculations and evaluated PESs in the light of TICT model using Gaussian 03 software. The ground state lowest energy optimized structure has been calculated at DFT level with B3LYP functional and 6-31++G(d,p) basis set and selective parameters are presented in Table 3. In the optimized geometry both the donor and acceptor groups are found to be planar with the benzene ring and are similar to its methyl ester compound MAPAME [11]. However in most of the reported donor–acceptor charge transfer systems the nitrogen group has been found to be twisted with respect to the benzene ring. Considering the TICT model, the positions of the computed absorption and emission bands for the ground state global minimum structure are shown in Table 4. The steady state absorption spectra of MAPAEE in hexane solvent appears with a strong band maximum at 333 nm (3.72 eV) and the weak one at 318 nm (3.89 eV) and the same band in acetonitrile at 351 nm (3.53 eV) and 318 nm (3.89 eV). The calculated vertical transition energies to the S_1 and S_2 states in vacuum at TDDFT/B3LYP/6-31++G(d,p) level (we may consider that the calculations in vacuum is almost equivalent to that in non-polar solvent) are 330 nm (3.75 eV) and 290 nm (4.27 eV), respectively, and that in acetonitrile solvent using PCM-TDDFT/B3LYP/6-31++G(d,p) method are 362 nm (3.42 eV) and 292 nm (4.24 eV), respectively. So the deviation between the calculated transition energy and experimental band position in hexane and in acetonitrile is only 0.03 eV and 0.11 eV, respectively. Calculations in vacuum and acetonitrile solution indicate that the absorption band maximum observed in the experiment corresponds to the S_1 state which has the larger calculated oscillator strength value ($f = 0.851$ eV), i.e., this transition is of π–π^* character. The molecular orbital picture of MAPAEE in the ground state support the nature of HOMO–LUMO transition is of π–π^* character (Fig. 5a and b). In MAPAEE, it is assumed that two types of twisting can be possible- (i) twisting along the donor (—NHMe) group (θ_1), (ii) twisting along the acceptor (- = —COOEt) (θ_2). For the construction of the energy curves, the geometry is kept frozen to the optimized ground state at any point and for any electronic state; the only variable parameter is the twist angle which has been varied from 0° to 100° with 10° increments. It is clear from Fig. 6 that along any of the twisting path both in vacuum and in acetonitrile the ground state shows a single well potential where orthogonal conformation, either due to twisting of donor or for twisting of acceptor is the saddle point. Along both the twisting path, both in vacuum and in acetonitrile solvent, the S_1 state shows an asymmetric double well potential, i.e., initially excited S_1 state yields another minimum in the potential energy surfaces at orthogonally twisted geometrical orientation (Fig. 6). Both the twisting paths predict the formation of TICT state from LE state by crossing through a small energy barrier. The calculated barrier is found to be higher in the gas phase (which is considered to be same as non-polar solvent) than in acetonitrile solvent. Therefore, in hexane solvent, the transformation from LE to CT is less favour and only LE emission is expected in non-polar solvents. On the

Table 2
Quantum yields and emission lifetime of MAPAEE in selective solvents

Solvent	α	ϕ_{total}	τ_1(ns)(α_1)	τ_2(ns)(α_2)	$\langle\tau\rangle$ (ns)	χ^2	$k_f \times 10^{-9}$ (s^{-1})	$k_{nr} \times 10^{-9}$ (s^{-1})
Hexane	–	1.3×10^{-2} (LE)	0.011(0.376)	0.013(0.624)	0.012	3.5	1.08	82.25
Acetonitrile	–	8.23×10^{-2} (CT)	0.027(1.00)	0.1(−0.035)	–	2.0	3.07	33.96
Ethanol	0.86	4.1×10^{-2} (CT)	–	–	–	–	–	–
Methanol	0.98	3.0×10^{-2} (CT)	0.016(0.07)	0.018(0.93)	0.017	1.0	1.76	57.05
Water	1.10	6.4×10^{-3} (CT)	–	–	–	–	–	–

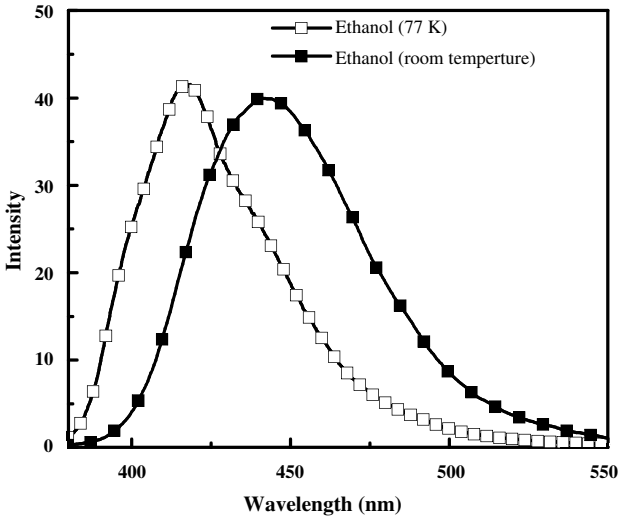

Fig. 4. Emission spectra of MAPAEE at 77 K in ethanol glass matrix and in ethanol solvent.

Table 3
Optimized geometry for the ground state of MAPAEE in vacuo using DFT (B3LYP/6-31++g(d,p)) method

Bond	Calculated values (Å)	Angle/dihedral angle	Calculated values (°)
R_{C1-C2}	1.410	∠N7—C1—C2	122.11
R_{C2-C3}	1.391	∠H20—N7—C1	117.47
R_{C3-C4}	1.407	∠C3—C4—C8	119.32
R_{C1-N7}	1.374	∠C11—O13—C14	116.26
R_{N7-H2O}	1.006	∠O13—C14—C15	107.62
R_{N7-C9}	1.447	∠C9—N7—C1—C2	0.00
R_{C4-C8}	1.454	∠H20—N7—C1—C6	0.00
R_{C8-C10}	1.351	∠C3—C4—C8—C10	0.00
$R_{C10-C11}$	1.470	∠O12—C11—O13—C14	0.00
$R_{C11-O12}$	1.221	∠C11—O13—C14—C15	180.00
$R_{C11-O13}$	1.361		
$R_{O13-C14}$	1.445		
$R_{C14-C15}$	1.517		

other hand polar solvent can tune this energy barrier and CT emission is expected through LE state excitation as the barrier is low. Along both the twisting paths, the calculated transition energy for the orthogonal twisted conformers is very close to the experimentally observed emission value (Table 4). In acetonitrile solvent the observed CT emission band is at 435 nm (2.91 eV) and the calculated transition energy due to orthogonal twisting of donor is 427 nm (2.90 eV) and that for twisting of acceptor is 421 nm (2.94 eV). The calculated oscillator strength values and molecular orbital picture support total decoupled nature of the interacting states in both the orthogonal orientations. Due to twisting of —NHMe group ($\theta_1 = 90°$), the CT excitation is characterized by n–π^* type transition ($f = 0.0$) (Fig. 5c and d), where as at the twisting of acceptor group ($\theta_2 = 90°$) (Fig. 5e and f), the single excitation is

Table 4
Computed parameters of MAPAEE in vacuum and acetonitrile solvents using DFT method with B3LYP hybrid functional and 6-31++g(d,p) basis set

Medium	State	Absorption		Emission		
		E_{th} (eV)	E_{ex} (eV)	E_{th}[a] (eV)	E_{th}[b] (eV)	E_{ex} (eV)
Vacuo	S_1	3.75	–	3.19	3.28	–
	S_2	4.27	–	4.20	4.23	–
Acetonitrile	S_1	3.42	3.53	2.90	2.94	2.91
	S_2	4.24	3.89	4.01	4.29	–

E_{th} is the calculated energy value ($E_{excited} - E_{ground}$) at DFT level (B3LYP/6-31++G(d,p)).
E_{ex} is the experimental value.
[a] Emission energy due to twisting of —NHMe group.
[b] Emission energy due to twisting of —CH=CH—COOEt group.

$\pi_{benzene}$–$\pi_{acceptor}$ type ($f = 0.0$). As seen in the molecular-orbital pictures shown in Fig. 5a and b, the nitrogen lone pair is found to be delocalized over the benzene ring in the HOMO of ground state optimized structure (Fig. 5a) and acceptor twisted geometry (Fig. 5e). On the other hand nitrogen lone pair is localized in the HOMO of donor twisted geometry (Fig. 5c). Therefore, it seems that delocalization of nitrogen lone pair over benzene ring does not support CT process along the twisting of acceptor site or in the un-twisted state. Where as the localized nitrogen lone pair supports CT process along the twisting of donor group as there are available lone pair at the nitrogen centre at donor twisted geometry.

3.4. Study of interaction of MAPAEE with BSA

Fig. 7a shows the change of emission characteristics of MAPAEE in Tris–HCL buffer of pH 7.0 with increasing BSA concentrations. In Tris–HCl buffer, MAPAEE exhibits the large red shifted ICT emission band originating from the polar CT emissive state. As seen in Fig. 7a, with increase of protein concentration the CT emission band of MAPAEE shifts to the blue with increase of intensity. The blue shift of the emission band indicates that the probe binds to the less polar hydrophobic interior part of protein compared to that of aqueous phase. A more rigid environment is also encountered by MAPAEE inside the protein. The non-radiative channels operative in the aqueous phase are less operative in the hydrophobic protein environment and hence the fluorescence intensity of MAPAEE increases with increasing protein concentration.

A quantitative estimate or the extent of binding of MAPAEE to BSA is determined using the Benesi–Hildebrand relation [35]. The binding or complexation equilibrium for the 1:1 complex can be expressed as

$$\text{MAPAEE} + \text{BSA} \overset{K}{\leftrightarrow} \text{Complex}$$

Benesi–Hildebrand relation for these types of complexation processes is expressed in terms of fluorescence intensity with the assumption that [BSA] >> [Complex], i.e., concentration of the complex is very low compared to that of the free protein. Hence, free protein concentration can be replaced by total protein concentra-

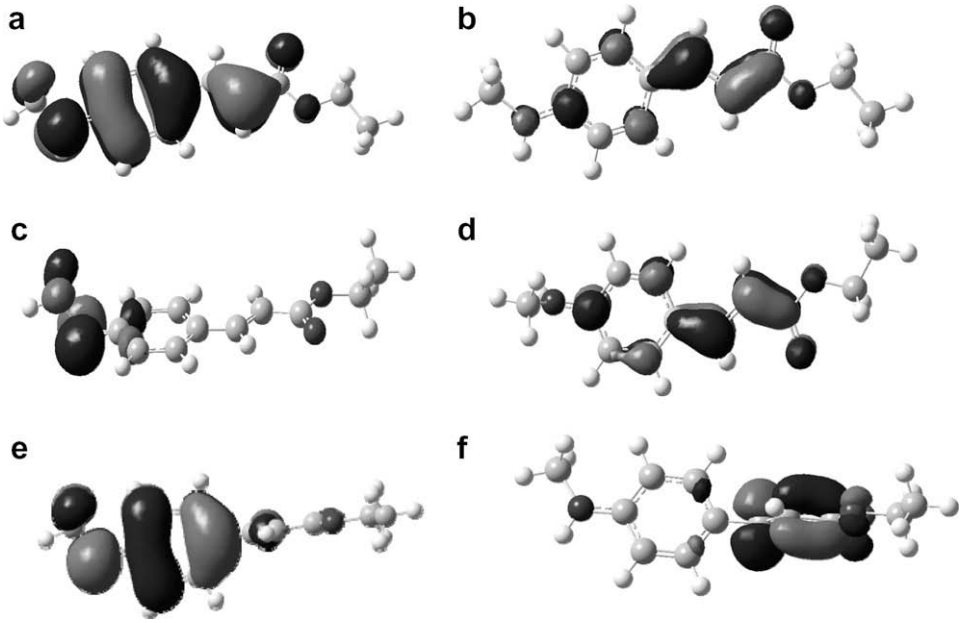

Fig. 5. Molecular orbital picture (a) HOMO of ground state optimized structure, (b) LUMO of ground state optimized structure, (c) HOMO of 90° twisted conformer at donor side, (d) LUMO of 90° twisted conformer at donor side, (e) HOMO of 90° twisted conformer at acceptor side, (f) LUMO of 90° twisted conformer at acceptor side.

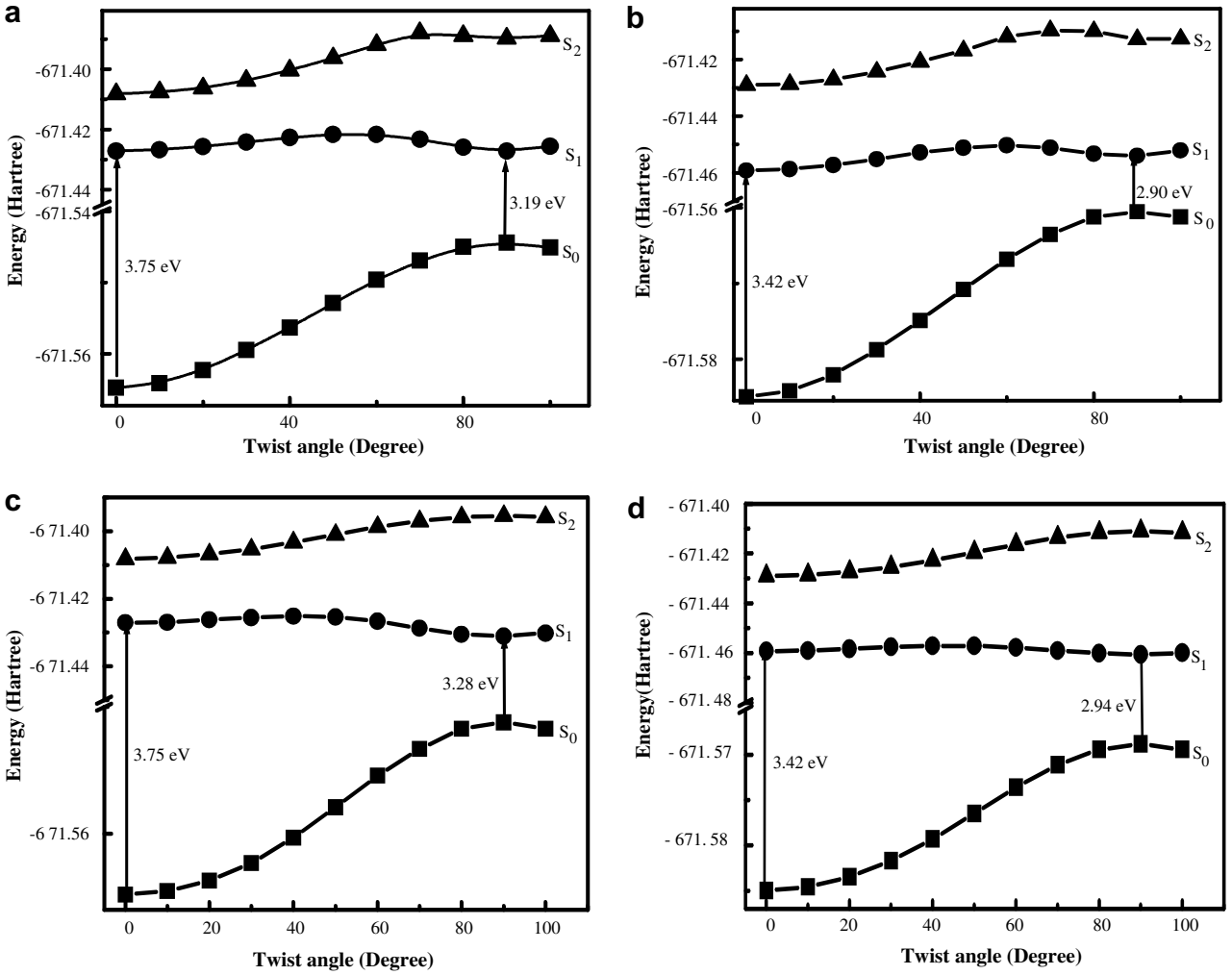

Fig. 6. Potential energy surfaces of MAPAEE along the twisting of (a) donor side in vacuum (θ_1), (b) donor side in acetonitrile (θ_1), (c) acceptor in vacuum (θ_2), (d) acceptor side in acetonitrile (θ_2).

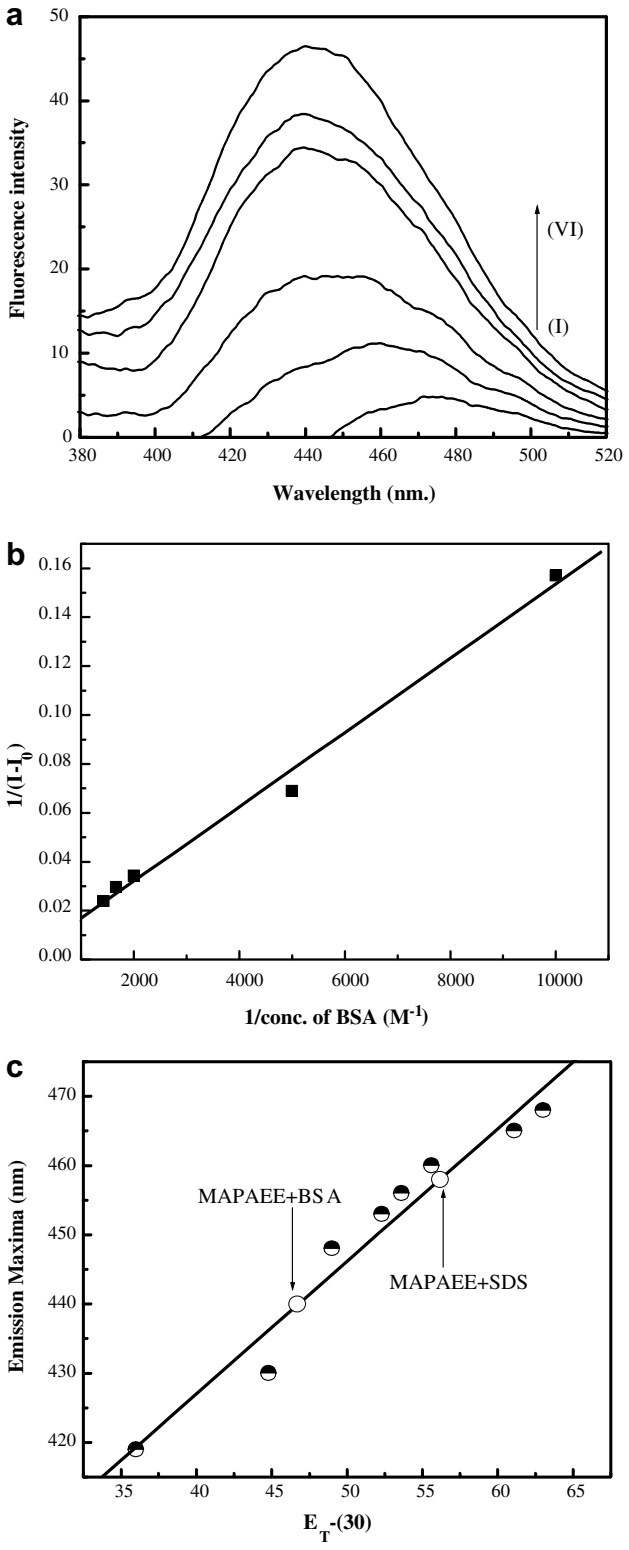

Fig. 7. (a) Emission of MAPAEE in (I): 0, (II):10, (III): 20, (IV): 50, (V): 60 and (VI): 70 μM BSA in Tris–HCl buffer (pH 7.0), (b) the Benesi–Hildebrand plot of $1/(I-I_0)$ vs. 1/[BSA], (c) calibration curve for micropolarity determination in proteinous and micellar environment: Plot of emission maxima of MAPAEE in water–dioxane mixtures against corresponding $E_T(30)$ values.

tion. The binding constant relation can be expressed by replacing the concentration of the components in terms of fluorescence intensity as

$$\frac{1}{(I-I_0)} = \frac{1}{(I_1-I_0)} + \frac{1}{(I_1-I_0)K[\mathrm{BSA}]}$$

where I_0, I and I_1 are the emission intensities in absence of, intermediate and infinite concentration of BSA, respectively. As seen in Fig. 7b, the plot of $1/[I-I_0]$ vs. 1/[BSA] shows a straight line indicating 1:1 complexation between MAPAEE and BSA. From the ratio of intercept and slope of Benesi–Hildebrand plot the extent of binding (K) is determined to be $0.818 \times 10^4\ \mathrm{mol}^{-1}$. The associated free energy change, ΔG, for the binding process was then calculated to be $-22.32\ \mathrm{kJ/mol}^{-1}$. The large binding constant indicates strong binding of the CT probe to the hydrophobic part of BSA protein and the free energy change favours spontaneous complexation process.

The blue shift of the CT band indicates that the micropolarity at the binding site of protein back bone is different from that of aqueous phase. Fluorescent probe techniques have been successfully used in determining the micropolarity of environments in proteins, micelles, cyclodextrin cavities etc. [36–41]. The Reichardt $E_T(30)$ scale [31] based on the transition energies of the ICT band of betaine dye in various solvent polarities has been widely used to estimate micropolarities of the environments [36–41]. Here we have attempted to get an idea about the local polarity of MAPAEE bound to BSA by using the $E_T(30)$ scale. As the position of the CT emission band of MAPAEE bound to BSA (440 nm) appears in between the position of the same band in dioxane (413 nm) and water (467 nm) it can be said that the micropolarity of the protein environment should definitely be in between the polarity of pure dioxane and pure water. The ICT emission of MAPAEE was monitored in various water–dioxane mixtures by comparing the position of the CT band of BSA bound MAPAEE with those in different water–dioxane mixtures of known $E_T(30)$ values. Fig. 7c shows a clear estimate of local polarity of the protein at the probe binding hydrophobic site. From the figure it is seen that the $E_T(30)$ is 46.7 and it is in between water and dioxane.

In the Fluorescence Resonance Energy Transfer (FRET) process a donor molecule is excited at its specific excitation wavelength and this molecule by dipolar interaction transfers the energy non-radiatively to an acceptor molecule lying within Förster distance of 2–8 nm from it. The efficiency of FRET depends on three parameters- (i) the distance between donor and acceptor must be within the specified Förster distance of 2–8 nm; (ii) there must be appreciable overlap between donor fluorescence and acceptor absorption band and (iii) proper orientation of the transition dipole of the donor and the acceptor fluorophore. According to Förster, the efficiency (E) of FRET process can be expressed by the following simple equation:

$$E = 1 - \frac{F}{F_0} \tag{1}$$

where E is the efficiency of energy transfer; F and F_0 are the fluorescence intensities of donor in presence and absence of the acceptor, respectively.

It is found that the emission curve of tryptophan of BSA overlap well with the absorption curve of the fluorescence probe MAPAEE. Therefore we have excited tryptophan at 280 nm and monitoring the emission of tryptophan ($\lambda_{em} = 350$ nm) and MAPAEE ($\lambda_{em} = 460$ nm). Fig. 8 shows the variation of fluorescence spectra of tryptophan of BSA with increasing concentration of probe MAPAEE. On gradual addition of MAPAEE it is seen that the intensity of tryptophan emission decreases with the emergence of a new band at ~460 nm. This implies that the radiation emitted by tryptophan of BSA is transferred to the probe MAPAEE by the process of FRET leading to an increase in emission intensity of the probe molecule. The efficiency of energy transfer from tryptophan to the fluorescence probe is found to be ~93%, i.e., the energy transfer efficiency from tryptophan to the probe is quite high. High FRET

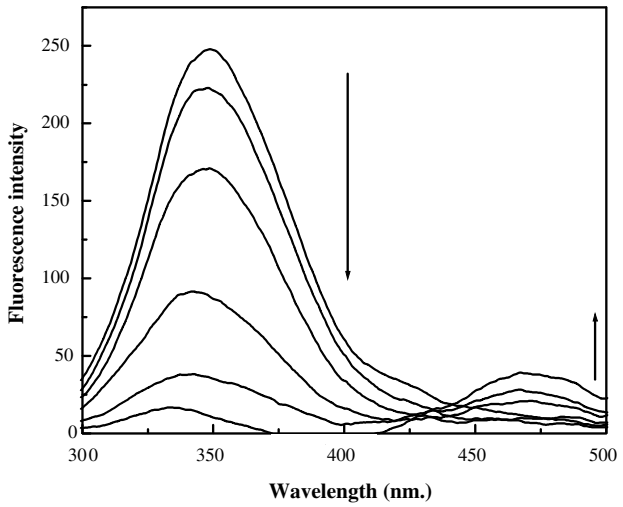

Fig. 8. Fluorescence spectra of tryptophan of BSA with an increasing concentration of MAPAEE. Arrow indicates increasing concentration of MAPAEE.

efficiency also supports the strong nature of binding of BSA with MAPAEE molecule.

3.5. Interaction of MAPAEE with SDS

ICT probes are being widely used by many workers to investigate interactions and/or local environments of bio-mimicking micellar aggregates [38,42–44]. The changes of the local environment that take place when the solvent polarity sensitive probe moves from the bulk aqueous phase to the micellar region in turn produce prominent changes in the spectral characteristics of the probe. We have seen that the red shifted emission maxima of MAPAEE has its origin in a polar charge transfer (CT) state. Even slight changes in polarity of the surrounding medium will then cause shifting of this ICT emission position which serves as a good way of to monitor micelle–MAPAEE interactions. Fig. 9a shows the effect of increasing SDS concentrations on the emission characteristics of MAPAEE. A clear blue shift of this maximum from 467 nm in water to 458 nm in 12 mM SDS is observed which is also accompanied with a simultaneous increase in emission intensity. Blue shift of the polarity sensitive ICT emission hints at a lowering of local polarity as the probe moves from the bulk aqueous phase to the micellar environment. Here again, we have interpolated the position of the emission maxima of MAPAEE in 12 mM SDS on the previously mentioned water–dioxane calibration curves for micropolarity determination (Fig. 7c). The polarity of the local micellar environment was then found to be 56.17 on the $E_T(30)$ scale. This value suggests that in SDS, MAPAEE is no longer resident in the highly polar aqueous phase ($E_T(30) = 63.1$) but rather encounters a local environment polarity which is somewhere in between the polarities of pure methanol ($E_T(30) = 55.4$) and pure water ($E_T(30) = 63.1$). However, this $E_T(30)$ value also suggests that in the SDS micelles MAPAEE does not encounter a microenvironment similar to non-polar alkanes. Hence, we can say that the probe does not penetrate deep into the hydrophobic core of the SDS micelle. Instead, in all probability, MAPAEE lies in the water-micelle interfacial region where it has been reported that the polarities of the local environment are usually in between those of pure water and pure alcohols [38].

Fig. 9b shows the variation CT emission intensity of MAPAEE with increasing concentrations of SDS. Correlation of ICT emission intensity with SDS concentrations follows two distinct lines, one for the surfactant concentrations before and one for the same after the critical micellar concentration (CMC). The CT emission increases steadily till 8 mM SDS concentration after which the increase becomes much less steep. The distinct break in these two lines occurs at 8 mM SDS concentration which is the reported CMC of SDS. Therefore, MAPAEE molecule could be used as a good fluorosensor for determination of CMC of micelles [43,44].

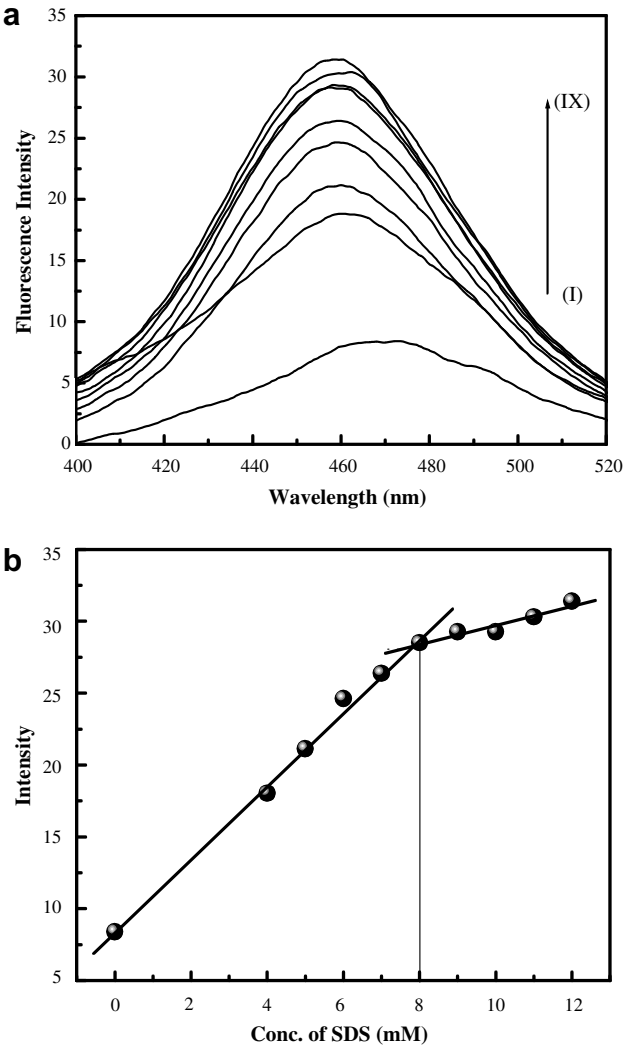

Fig. 9. (a) Variation of emission characteristics of MAPAEE with increasing surfactant (SDS) concentrations: (I) 0, (II) 4, (III) 5, (IV) 6, (V) 7, (VI) 8, (VII) 9, (VIII) 10 and (IX) 11 mM SDS concentration, (b) plot of intensity of emission maxima of MAPAEE against SDS concentration.

4. Conclusion

The photophysical properties of MAPAEE have been investigated in different solvent by absorption and emission measurement in combination with DFT calculations and all spectral findings are similar to that of its methyl ester compound, i.e., the change of ester group from methyl to ethyl does not change spectral characteristics. The molecule clearly shows excited state intramolecular charge transfer reaction characterized by solvent polarity dependent red shifted emission band. In protic solvent the molecule forms intermolecular hydrated clusters which facilitate ICT process. Theoretical calculations predict the formation of a stabilized twisted intramolecular charge transfer state by twisting both the donor and acceptor groups. Although, there is a barrier along the twisting coordinates, but the emission spectra in presence of acid and localized lone pair at the donor twisting geometry

support that the twisting of donor group may be responsible for the solvent dependent Stokes shifted emission. The solvent polarity dependent CT emission band is used as fluorosensor to determine local micropolarity of protein and micellar medium. Spectral modulation of MAPAEE in presence of BSA well reflects the nature of binding of probe to protein hydrophobic back bone and fluorescence resonance energy transfer process. It is also used as sensor to determine $E_T(30)$ polarity parameter and critical micellar concentration of SDS micellar aggregates.

Acknowledgements

N.G. acknowledges DST, India (Project No. SP/S1/PC-1/2003) and CSIR, India (Project No. 01(2161)07/EMR-II, Dt. 24.10.2007) for financial support. The authors thank Prof. T. Ganguly of IACS, Kolkata for allowing them low temperature measurement and Prof. Periasamy and G. Krishnamoorthy and Ms. Madhuri of T.I.F.R, Mumbai for lifetime measurement.

References

[1] E. Lippert, W. Luder, H. Boos, in: A. Mangini (Ed.), Advances in Molecular Spectroscopy, Pergamon Press, Oxford, 1962, p. 443.
[2] K. Rotkiewicz, K.H. Grellmann, Z.R. Grabowski, Chem. Phys. Lett. 19 (1973) 315.
[3] U. Leinhos, W. Kuhnle, K.A. Zachariasse, J. Phys. Chem. 95 (1991) 2013.
[4] A.L. Sobolewski, W. Domcke, Chem. Phys. Lett. 259 (1996) 119.
[5] A.-D. Gorse, M. Pesquer, J. Phys. Chem. 99 (1995) 4039.
[6] K. Rotkiewicz, W. Rettig, J. Lumin. 54 (1992) 221.
[7] K.A. Zachariasse, T. Von der Haar, A. Hebecker, U. Leinhos, W. Kuhnle, Pure Appl. Chem. 65 (1993) 1745.
[8] V.A. Galievsky, S.I. Druzhinin, A. Demeter, Y.-B. Jiang, S.A. Kovalenk, L.P. Lustres, K. Venugopal, N.P. Ernsting, N.P. Allonas, M. Noltemeyer, R. Machinek, K.A. Zachariasse, Chem. Phys. Chem. 6 (2005) 2307.
[9] A. Chakraborty, S. Kar, N. Guchhait, Chem. Phys. 324 (2006) 733.
[10] A. Chakraborty, S. Kar, N. Guchhait, J. Phtochem. Photobiol. Chem. A 181 (2006) 246.
[11] A. Chakraborty, S. Kar, D.N. Nath, N. Guchhait, J. Phys. Chem. A 110 (2006) 12089.
[12] C.J. Jodicke, H.-P. Luthi, J. Am. Chem. Soc. 125 (2003) 252.
[13] R. Cammi, B. Mennucci, J. Tomasi, J. Phys. Chem. A 104 (2000) 5631.
[14] Z.I. Cai, J.R. Reimers, J. Chem. Phys. 112 (2000) 527.
[15] O.V. Gritsenko, S.J.A. van Guibergen, A. Gorling, E.J. Baerends, J. Chem. Phys. 113 (2000) 8478.
[16] X.-H. Duan, X.-Y. Li, R.-X. He, X.-M. Cheng, J. Chem. Phys. 122 (2005) 084314.
[17] C.J. Jodicke, H.-P. Luthi, J. Chem. Phys. 119 (2003) 12852.
[18] C.J. Jodicke, H.-P. Luthi, J. Chem. Phys. 117 (2002) 4146.
[19] M. J. Frisch et al., Gaussian 03, Revision B.03, Gaussian, Inc., Pittsburgh PA, 2003.
[20] M.E. Casida, K.C. Casida, D.R. Salahub, J. Quant. Chem. 70 (1998) 933.
[21] J. Neugebauer, O. Gritsebko, E. Jan Baerends, J. Chem. Phys. 124 (2006) 214102.
[22] D. Jacquemin, M. Bouhy, E.A. Perpete, J. Chem. Phys. 124 (2006) 204321–204329.
[23] H.H. Jaffe, M. Orchin, Theory and Application of Ultraviolet Spectroscopy, Wiley, New York, 1962.
[24] A. Chakraborty, S. Kar, N. Guchhait, Chem. Phys. 320 (2006) 75.
[25] C. Cazeau-Dubroca, S. Ait Lyazidi, P. Cambou, A. Peirigua, P.H. Cazeau, M. Pesquer, J. Phys. Chem. 93 (1989) 2347.
[26] Y. Kim, M. Yoon, Bull. Korean Chem. Soc. 19 (1998) 980–985. and the references therein..
[27] R.L. Cukier, J. Phys. Chem. 98 (1994) 2377. and the references therein..
[28] J. R Lakowicz, Principles of Fluorescence Spectroscopy, second ed., Kluwer Academic, Hongham, 1999.
[29] S. Sumalekshmy, K.R. Gopidas, J. Phys. Chem. B 108 (2004) 3105.
[30] N. Mataga, Y. Kaifu Koizumi, Bull. Chem. Soc. Jpn. 29 (1956) 465.
[31] C. Reichardt, Chem. Rev. 94 (1994) 2319.
[32] R.W. Taft, M. Kamlet, J. Am. Chem. Soc. 98 (1976) 2886.
[33] M. Maus, W. Rettig, D. Bonafoux, R. Lapouyade, J. Phys. Chem. A 103 (1999) 3388.
[34] F.D. Lewis, W. Weigel, J. Phys. Chem. A 104 (2000) 8146.
[35] M.L. Benesi, J.H. Hildebrand, J. Am. Chem. Soc. 71 (1949) 2703.
[36] R. Das, D. Guha, S. Mitra, S. Kar, S. Lahiri, S. Mukherjee, J. Phys. Chem. A 101 (1997) 4042. and the references therein..
[37] A. Chakraborty, A. Mallick, B. Haldar, P. Das, N. Chattopadhyay, Biomacromolecules 8 (2007) 920.
[38] P. Das, A. Chakraborty, A. Mallick, N. Chattopadhyay, J. Phys. Chem. B 111 (2007) 11169. and references therein..
[39] F.-Y. Wu, Z.-J. Ji, Y.-M. Wu, X.-F. Wan, Chem. Phys. Lett. 424 (2006) 387.
[40] S. Kundu, N. Chattopadhyay, J. Photochem. Photobiol. Chem. A 88 (1995) 105.
[41] S. Kundu, N. Chattopadhyay, J. Mol. Struct. 344 (1995) 151.
[42] A. Chakraborty, P. Das, A. Mallick, N. Chattopadhyay, J. Phys. Chem. B 112 (2008) 3684.
[43] G. Krishnamoorthy, S.K. Dogra, Chem. Phys. Lett. 323 (2000) 234.
[44] S. Kundu, S. Maity, S.C. Bera, N. Chattopadhyay, J. Mol. Struct. 405 (1997) 231.